Model-guided Segmentation of Corpus Callosum in MR Images

Arvid Lundervold[1], Nicolae Duta[2], Torfinn Taxt[1] & Anil K. Jain[2]

[1]*Section for Medical Image Analysis and Informatics, Department of Physiology*
University of Bergen, Årstadveien 19, N-5009 Bergen, Norway E-mail: Arvid.Lundervold@pki.uib.no
[2]*Department of Computer Science and Engineering, Michigan State University, East Lansing, MI 48824-1226, USA*

Abstract

Magnetic resonance imaging (MRI) of the brain, followed by automated segmentation of the corpus callosum (CC) in midsagittal sections has important applications in neurology and neurocognitive research since the size and shape of the CC are shown to be correlated to sex, age, neurodegenerative diseases and various lateralized behavior in man. Moreover, whole head, multispectral 3D MRI recordings enable voxel-based tissue classification and estimation of total brain volumes, in addition to CC morphometric parameters. We propose a new algorithm that uses both multispectral MRI measurements (intensity values) and prior information about shape (CC template) to segment CC in midsagittal slices with very little user interaction. The algorithm has been successfully tested on a sample of 10 subjects scanned with multispectral 3D MRI, collected for a study of dyslexia. We conclude that the proposed method for CC segmentation is promising for clinical use when multispectral MR images are recorded.

1 Introduction

Several studies indicate that the size and shape of the *corpus callosum* (CC) in human brain are correlated to sex [1, 8, 29], age [29, 37], brain growth and degeneration [15, 23], handedness [6], and to various types of brain dysfunction [9, 10, 18, 28, 30]. In order to find such correlations in living brains, magnetic resonance imaging (MRI) is regarded as the best method to obtain cross-sectional area and shape information from *corpus callosum* (Fig. 1). In addition, MRI is fast and safe, without any radiation exposure to the subject such as with X-ray CT. Since manual tracing of *corpus callosum* in MR images is time consuming, operator-dependent, and does not directly give quantitative measures of cross-sectional areas or shape, there is a need for automated and robust methods for localization, delineation and shape description of the *corpus callosum*.

We propose a new algorithm that uses both the prior information about shape (CC template) and multispectral MRI measurements (intensity values) to segment CC in midsagittal slices with very little user interaction. The algorithm takes advantage of the multispectral properties of MRI, which we use in low-level tissue classification, and the typical appearance in midsagittal slices of a simply closed curve, which we represent as a dynamic contour interacting with the low-level segmentation.

We see several advantages with the proposed method compared to other CC segmentation methods. (i) Our method is almost fully automated. For a given subject, the only user interaction is to pick the midsagittal slice by visual inspection. (ii) Computational requirements are small, with a CPU time of about 2 s/slice for low-level segmentation on a SGI Indigo2 R10000 workstation. Matching and final clean-up takes 10 s/image on the average. (iii) From experiments on clinical MRI data from 10 subjects, the method gives robust and accurate CC segmentation results when compared to manual tracings. (iv) Our low-level segmentation step, which uses multispectral MR data, can be directly applied to all the slices in the data set [22]. This enable whole brain volume estimates of gray matter, white matter and cerebrospinal fluid to be compared to CC morphometric parameters.

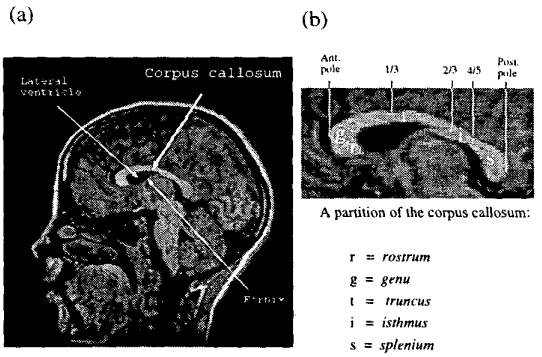

Figure 1: (a) Midsagittal, T1-weighted MRI section of the brain (12 year old boy) showing the *corpus callosum* as a C-shaped central structure with high signal intensity. (b) Details showing a partition of the *corpus callosum*. Ant. = anterior; Post. = posterior

The rest of the paper is organized as follows. In Section 2 we present current methods reported in the literature for shape analysis of anatomical structures in medical im-

0-7695-0149-4/99 $10.00

ages. Our new algorithm, that uses both prior information about shape (CC template) and multispectral MRI measurements (intensity values), is described in Section 3. Experimental results, testing the algorithm on a sample of 10 multispectral 3D whole-brain acquisitions, are reported in Section 4. Section 5 concludes the paper with a discussion of clinical applicability and possible improvements of the proposed method.

2 Previous Work

Manual tracing of the CC boundary in midsagittal MR images seems to be the most frequently used method in clinical studies of CC morphometry (e.g., [1, 7, 15, 18]).

Dynamic contour models have been used to segment various structures in the brain and other parts of the body imaged with MRI or X-ray CT (see, e.g., [24] for a survey). Staib & Duncan [31] introduced a probabilistic deformable model, based on the elliptic Fourier decomposition of the boundary, to segment the *endocardium* and the *epicardium* boundaries of the left ventricle in cardiac MR images and the boundary of the *corpus callosum* in midsagittal MR images. They succeeded in delineating the CC structure using six harmonics, but their direct search optimization method was slow and the final CC contour was visually inaccurate.

Szekely et al. [32] segmented corpus callosum from gray-valued MRI images using constrained elastic deformations of a flexible Fourier contour model. The algorithm requires selection of an anatomically defined reference coordinate system where the AC/PC line has to be determined manually.

Ghanei and coworkers [13] segmented the hippocamus using a discrete contour representation and adaptive internal force weights. However, their method is dependent on manual placement of an initial polygon close to the target boundary. Further, several parameters need to be specified by the user.

Various statistical shape models with parameterization based on Fourier descriptors, wavelet descriptors and on a set of labeled points were developed by Neumann & Lorenz [25] and applied to detect the closed contour of spinal vertebra in single axial slices from 3D CT data. Their method requires the user to mark points interactively on the segmented contour. The results are sensitive to the normalization procedure being used for shape parameterization regarding translation, rotation and scaling.

An interactive live-wire boundary extraction method was proposed by Barrett & Mortensen [2], where boundary detection was formulated as a graph searching problem. Their local cost function incorporates Laplacian zero-crossing, gradient magnitude and gradient direction, and the goal is to find the globally minimum cumulative cost path between a start node (pixel) and a set of goal nodes. The method enables fast detection of the outer boundary of the brain in MRI, but requires intensive user interaction and suffers from some degree of intra-observer and inter-observer variability.

Vemuri et al. [36] have developed fast numerical algorithms for fitting multiresolution hybrid shape models to brain MRI. Their shape model is described globally as a deformable superquadric geometry in a wavelet basis and locally by a triangular finite-element discretization, where fitting is regarded as an energy minimization problem. However, data points have to be placed on the boundary of interest or a rough model initialization has to be traced by the user. Moreover, the model fitting was not accurate when applied to caudate nucleus or the hippocampus. Since their algorithm can be used without prior knowledge of the shape of interest, it is suited for the learning phase, enabling fast automatic construction of prior shape models.

Lundervold & Storvik [21] proposed a method to segment brain parenchyma and cerebrospinal fluid spaces in multispectral axial MR images of the head. The two-stage algorithm, formulated in a Bayesian framework, combines multispectral tissue signal intensities and anatomical shape information. Each tissue type is represented by a multivariate Gaussian, and *a priori* knowledge of gross brain anatomy is described by a stochastic region boundary model. The algorithm performed well in most of the 10 data sets tested. However, due to iterative parameter updating and simulated annealing optimization the algorithm is slow. Moreover, since the fornix and the CC are connected structures, both representing white matter, their algorithm might not be suitable in our case.

Duta & Sonka [11] designed a knowledge-based active shape procedure (cfr. [5]) that incorporated *a priori* knowledge about the objects of interest and their specific structural relationships in order to provide robust segmentation and labeling. Their model was successfully used to identify ten neuroanatomic structures in MR brain images.

Directly related to our application, Davatzikos and coworkers [8] proposed an elastic deformation transformation that normalizes *corpus callosum* into Talairach space [33]. The properties of this transformation was then used as a quantitative description of CC shape with respect to the Talairach atlas, providing a common reference system for intersubject comparisons. In their two-stage algorithm, boundary points of the CC are initially extracted by seeded region growing in the midsagittal MR image of the subject's head and in the photographed and digitized Talairach image. An active contour algorithm is then applied to both boundaries. In the second stage, an elastic deformation transformation warps the atlas image and brings its CC contour into registration with the CC contour in the subject. The algorithm requires little user intervention. However, the method is CPU demanding and point correspondence between homologous points on each active contour is not guaranteed. Using the algorithm on midsagittal MR image

from a sample of eight women and eight men, they found a greater splenial area in females than males.

Bookstein [4] has introduced a combination of Procrustes analysis and thin-plate splines for multivariate comparison of the shape outlines. The method was applied to the *corpus callosum* boundary in midsagittal MR images from 12 normals and from 13 patients with schizophrenia. Using his algorithm, he also reanalyzed the sample of 16 individuals reported in [8], and found a statistically significant CC shape difference between the sexes, primarily a vertical extension of the splenium in females compared to males.

3 Proposed Method

We use a combination of a bottom-up (multispectral contextual classification) and a top-down (shape-matching) approach to localize and segment *corpus callosum*, illustrated in Fig. 2. Top down segmentation is guided by prior knowledge about position and shape of *white matter*, the only tissue type of *corpus callosum*. If shape-matching was applied directly to the entire image, the segmentation process would be substantially slower and not accurate enough with local details. On the other hand, a preliminary bottom up segmentation improves the speed by eliminating much of the unneeded information from the image (in our case information about gray-level structures) while a final bottom-up morphological cleaning improves local accuracy.

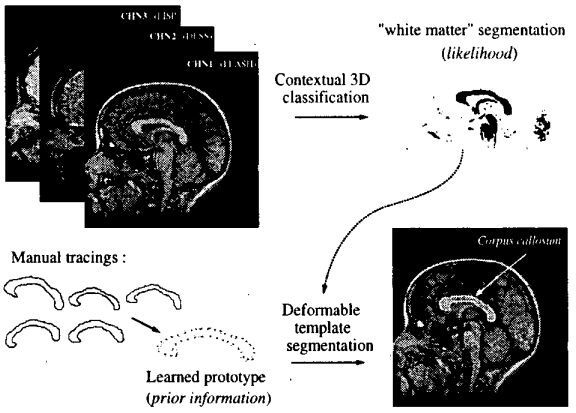

Figure 2: Integration of bottom-up voxel classification and top-down deformable template segmentation.

3.1 Low-level Segmentation

A multispectral and contextual tissue classification algorithm is used to obtain an initial segmentation of the brain MR image.

Training Technique We use multivariate normal densities f_k with tissue specific mean vectors and covariance matrices, since this model is simple and is shown to be reasonable in other MRI recordings from the brain [35]. To obtain tissue-specific parameter estimates (mean values and covariance matrices of the class-conditional densities), we used K-means partitional clustering [19] of the voxels in a *single* 2D slice recorded in one of the subjects with subsequent manual labeling [34, 35]. The numbers of clusters were selected to match the expected number of normal tissue types present in the imaged anatomy.

To reduce the number of voxels to be clustered, a mask was drawn manually around the central part of the head. This mask was also used to restrict classification of the seven central multispectral slices in all other subjects in the study.

3D Contextual Classification To perform a statistical classification of the central multispectral slices in each subject, we used a 3D generalization of Haslett's contextual classification scheme [16] with a first-order, 3D neighborhood [17, 20]. Let $y = (y_1, \ldots, y_N)$ denote the N voxel-based pattern vectors (i.e., measured signal intensities within a region of interest) which are to be labelled $C_1, \ldots, C_N$, where C_k belongs to one of the K predefined tissue types. For each voxel i, we want to compute $C_i^\star = \arg\max_k P(C_i = k|y)$, the maximum *a posteriori* probability. *Non-contextual* classification model make use of the signal intensity only of the voxel of interest, i.e., $P(C_i = k|y) = P(C_i = k|y_i)$, where $P(C_i = k|y)$ is computed as follows:

$$P(C_i = k|y) = P(C_i = k|y_i) = \frac{\pi_k f_k(y_i)}{\sum_{k=1}^{K} \pi_k f_k(y_i)},$$

and f_k is the probability density distribution for class k and π_k is the *a priori probability* of class k.

In our *contextual* classification model we make additional use of measurements in a spatial neighborhood, ∂_i, of pixel i that is $P(C_i = k|y) = P(C_i = k|\partial_i)$. In Haslett's extended model, the equation for computing $P(C_i = k|\partial_i)$ is:

$$P(C_i = k|\partial_i) = P(C_i = k|y_i, y_{iS}, y_{iN}, y_{iE}, y_{iW}, y_{iD}, y_{iU}) =$$

$$\frac{\pi(k) f_k(y_i) T_k(y_{iS}) T_k(y_{iN}) T_k(y_{iE}) T_k(y_{iW}) T_k(y_{iD}) T_k(y_{iU})}{\sum_{k=1}^{K} \pi(k) f_k(y_i) T_k(y_{iS}) T_k(y_{iN}) T_k(y_{iE}) T_k(y_{iW}) T_k(y_{iD}) T_k(y_{iU})},$$

where

$$T_k(y_j) = \sum_{l=1}^{K} \pi(l|k) f_l(y_j)$$

and $\pi(l|k)$ is the transition probability of having class l in a voxel given that its neighbor is k, and iS, iN, IE, iW, iD, iU denote the six first-order neighbors of i on a 3D lattice (Fig. 3).

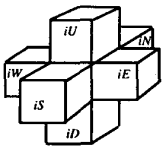

Figure 3: The six first-order neighbors of voxel i.

For simplicity, non-informative prior probabilities, $\pi_k = \frac{1}{K}$ $(k = 1, \ldots, K)$ and the default transition probabilities, $\pi(k|l) = \frac{0.1}{(K-1)}$ if $k \neq l$ and $\pi(k|l) = 0.9$ if $k = l$ $(k, l = 1, \ldots, K)$ were selected. Since the classification result is used only to guide the initial contour of the deformable model, no doubt or outlier options were used.

3.2 Deformable Model

Since CC has a relatively homogeneous gray-level interior, the main characteristic that makes it distinguishable from other structures in the brain is its shape. Therefore, we propose to learn the CC shape from the available manual tracings and use it in a model-based segmentation guided by the results of the low-level pixel classification.

The shape learning stage consists of automatically extracting a shape prototype (mean-shape) and its principal modes of variation from the given training set (Fig. 2). To compute the prototype, we first align the shapes from the training set into a common parameterization framework by selecting from every manual contour a subset of registered points of equal cardinality. This is achieved by performing a pair-wise alignment (using a least-squares type distance [3]) of a smoothed version of each shape to every original shape in the training set. The alignment procedure, somewhat resemblant to that of Feldmar and Ayache [12], first performs a global similarity registration of the two shapes, then refines it by applying a set of local alignments in a topological neighborhood (of each point) defined according to the natural point ordering along the contour. In this way, we obtain a pseudo-distance matrix whose entries are normalized alignment errors between every couple of shapes in the training set. The smoothed shape that has the smallest distance to the remaining ones (which can be considered a *best fit* to the training set) is used to extract from each training shape registered sets of corresponding points. Then, the mean shape is derived by Procrustes Analysis [14] applied to the previously extracted sets.

The deformable template segmentation step tries to warp the learned CC prototype onto the edges of the image obtained by low-level classification. In order to achieve a fast segmentation, we do not use the entire edge map from the low-level classification image. Instead, we first construct a region of interest defined in a coordinate system bounded by the anatomy. We found that simple thresholding can find the position (leftmost, rightmost and uppermost points) of the skull. We define a rectangular box with respect to this coordinate system that contains the CC in all the images (Fig. 4). We further simplify the task by morphological cleaning this region of interest. An erosion followed by a dilation procedure eliminates all small clusters (of pixels) from the region of interest. The borders of the remaining large clusters are computed and the CC prototype is registered and then warped to this edge image. Although in principle, the warping could be applied to the edge set obtained directly from the gray-level image, we found that the low-level classification eliminates most of the noisy edges belonging to other structures than CC.

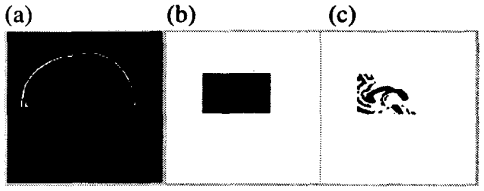

Figure 4: Region of interest. (a) Skull detection by thresholding. (b) ROI from the original FLASH image. (c) ROI from the "white matter" image.

4 Data and Experimental Results

MRI data We used a sample of 10 subjects scanned with MRI, selected from a larger database collected for a study of dyslexia. There were 5 boys, 10-12 years old, with well-characterized dyslexia and 5 boys with normal reading abilities. The MRI examinations were done on a 1.0 T Siemens Impact magnetom using whole head, multispectral 3D gradient echo acquisitions (Fig. 5): T1W FLASH TR=22ms, TE=6ms, FA=30°; T2W DESS TR=26, TE=9,45, FA=40; PDW FISP TR=23, TE=10, FA=15; FOV=256mm, 3D slab=160mm, 128×128×256 sagittal acquisition matrix. Each voxel has thus an extension of $1 \times 1 \times 1.25$ mm^3. The selection of the three pulse sequences (3D FLASH, DESS and FISP) was based on previous experimental results on the whole head tissue classifications using a set of 5 different 3D pulse sequences which used the same training procedure and contextual 3D classifier [22].

4.1 Tissue-specific Training

In low-level segmentation we used $K = 9$ classes to describe the different tissue types in the head. The tissue labels and their channel-specific mean values obtained from the training procedure are shown in Table 1. Note that the training was done in only one multispectral slice from a single subject in the sample. The estimated multivariate normal tissue-specific probability densities were then used in automated classification of the 7 central slices from each of the 10 subjects.

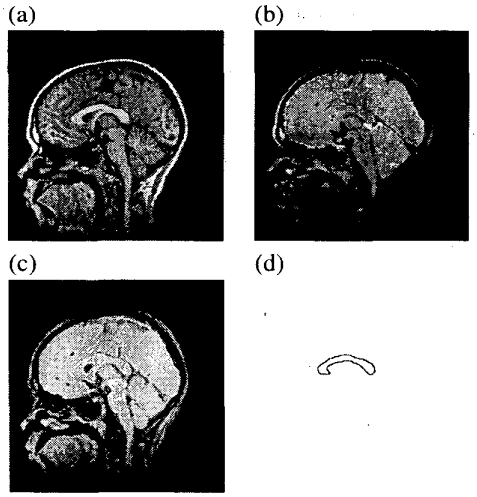

Figure 5: Multispectral slice (`slice066`) selected to represent the *corpus callosum* in subject #1-tj. (a) FLASH. (b) DESS. (c) FISP. (d) Manual tracing of *corpus callosum* using the FLASH channel.

k	Class name	No. of training samples	Mean (chn1)	Mean (chn2)	Mean (chn3)
1	muscle	916	172.3	64.6	86.9
2	fat	542	263.4	110.6	115.2
3	air-bone	7706	13.1	17.4	18.5
4	conn1	2881	90.5	65.4	118.5
5	conn2	3164	58.5	42.1	58.0
6	conn3	2903	76.8	112.5	140.9
7	white-m	3118	152.4	127.3	204.8
8	gray-m	7251	114.9	121.4	187.3
9	CSF	687	62.2	190.3	132.2

Table 1: Tissue classes and mean vectors computed from the training set (slice065 in subject #1-tj) used in all subsequent classifications. *conn1*, *conn2*, *conn3* denote different types of connective tissue and tissues representing partial volume effects. *white-m* = white matter, *gray-m* = gray matter.

4.2 Low-level Segmentation of White Matter

For each subject, the location of the central (midsagittal) slice was determined manually. Pixels classified as *white matter* in the selected slice from 6 of the subjects, using our 3D contextual classification rule, are shown in Fig. 6. Only the *white matter* segmentation was used as input to the shape matching algorithm since it is the only tissue type of the *corpus callosum*. From Fig. 6 we see that several anatomical structures apart from the *corpus callosum* were classified as *white matter*. Most prominent are the brain stem, the cerebellum (Fig. 6e) and the medial parts of the frontal lobe (Fig. 6a) and the occipital lobe (Figs. 6a, b, d-f). These latter areas are actually projections of the *corpus callosum* into the neocortical areas of the sectioned hemisphere.

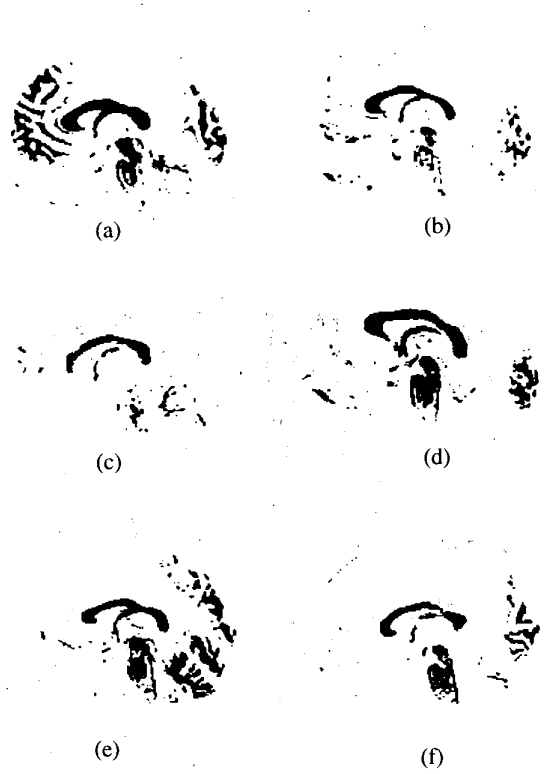

Figure 6: 3D classified 'white matter' including *corpus callosum* from 6 individuals using contextual classifier. (a) Subject #1-tj. (b) Subject #2-hb. (c) Subject #3-sj. (d) Subject #4-ah. (e) Subject #7-na. (f) Subject #9-pe.

In every subject there is also a smaller C-shaped structure located beneath the *corpus callosum* and connected to it. This is the *fornix*, a massive fibre bundle mainly containing projection fibres from the hippocampus and the subiculum. Since *fornix* is connected to CC, it needs to be separated. After morphological cleaning of the region of interest this was done at the shape matching stage where the learned CC prototype was warped to the eroded *white matter* segmentations.

4.3 Shape Matching and Final CC Segmentation

Fig. 7 shows the Procrustes average of the 5 manually traced CC shapes with the *scatter of fits* (as defined in [4]) overlaid. Consecutive point clouds are drawn in different gray-levels to prove that the clouds are non-overlapping, that is, the registration is precise.

Final segmentation results in 6 individuals from the complete set are shown in Fig. 8. The agreement between the manually traced "true" contours (not shown) and the computed contours was visually excellent in all 10 subjects. However, no shape distance metric was calculated to quantify the agreement.

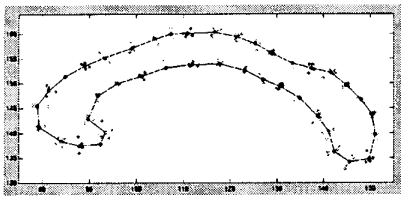

Figure 7: Automatic Procrustes average of the 5 CC shapes with the scatter of the points from the aligned examples.

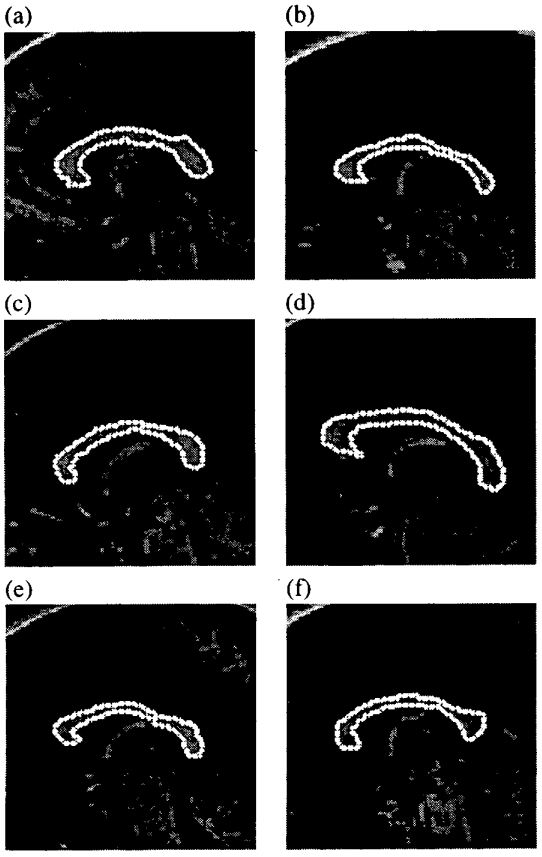

Figure 8: Segmentation results from 6 individuals. CC shape (white contour) in midsagittal T1-weighted FLASH channel image. (a) Subject #1-tj. (b) Subject #2-hb. (c) Subject #3-sj. (d) Subject #4-ah. (e) Subject #7-na. (f) Subject #9-pe.

5 Summary and Conclusions

In order to detect and segment the *corpus callosum* outline in midsagittal MR images for morphometric analysis, we have proposed a new algorithm that uses both prior information about shape (CC template) and the multispectral MRI measurements (intensity values), with little user interaction. The method has been successfully applied to 10 subjects with very good agreement between the manually traced ("true") outline and the detected outline. However, if the present choice of midsagittal section and the resulting CC segmentation will be used to calculate CC morphometry in each individual, one caution should be made. The reliability of callosal area and shape measurements is partly dependent on the method used for segmenting the CC boundary and partly dependent on the CC appearance in the slice selected to represent CC in a given subject. Relating to the last factor of variability, Rauch and Jinkins [27] studied the effect of subject placement in the scanner. Using 12 healthy subjects they found that the variability in cross-sectional area, attributable to differences in the orientation of the scan plane used to generate the midsagittal image was in the order of $\pm$ 3.7%. Variability in CC cross-sectional areas due to intra-observer measurement variation was found to be about $\pm$ 2.5%, using multiple sessions with manual tracing in a given image. To eliminate the need for uniformity of head position at the time of imaging, Semrud-Clikeman et al. [30] acquired T1-weighted 3D-SPGR images which were reformatted into a positionally normalized sagittal scan using proper rigid-body translation and rotation and subsequent re-slicing into 1.0 mm sagittal slices prior to morphometric analysis.

Although our segmentation results were visually good, the set of processed images is small. A natural next step will therefore be to evaluate quantitatively, on a larger data set, the present method against other approaches with respect to computation time, degree of robustness and accuracy. There are several good candidates for a comparative study. One such algorithm is gradient vector flow [38] using snakes and external force computed as a diffusion of the gradient vectors of a gray-level or a binary edge map derived from the sagittal MR image. This snake method has been shown to move snakes into boundary cavities which is a typical characteristic of the CC contour. Other methods which should be considered are the flexible Fourier contour model by Szekely and coworkers [32], the edge-focusing algorithm by Raman et al. [26], and also the contour deformation method developed in [8].

Acknowledgments

We thank Dr. Einar Heiervang for providing the data as part of his study of dyslexia, and Dr. Lars Ersland and Mr. Roger Barndon for technical assistance. A. K. Jain's research was supported by a grant from U.S. Norway Fulbright Foundation for Educational Research.

References

[1] L. S. Allen, M. F. Richey, Y. M. Chain and R. A. Gorski (1991). Sex differences in the corpus callosum of the living human being. *Journal of Neuroscience*, Vol. 11, pp. 933-942.

[2] W. A. Barrett and E. N. Mortensen (1997). Interactive live-wire boundary extraction. *Medical Image Analysis*, Vol. 1, pp. 331-341.

[3] P. Besl and N. McKay (1992). A method for registration of 3-D shapes. *IEEE Trans PAMI*, Vol. 14, pp. 239-256.

[4] F. Bookstein (1997). Landmark methods for forms without landmarks: morphometrics of group differences in outline shape. *Medical Image Analysis*, Vol. 1, pp. 225-243.

[5] P. E. Cootes, A. Hill, C. J. Taylor, and J. Haslam (1994). Use of active shape models for locating structures in medical images. *Image and Vision Computing*, Vol. 12, pp. 355-366.

[6] P. E. Cowell, A. Kertesz, and V. H. Denenberg (1993). Multiple dimensions of handedness and the human corpus callosum. *Neurology*, Vol. 43, pp. 2353-2357.

[7] P. A. Cowell, L. S. Allen, A. Kertesz, N. S. Zalatimo, and V. H. Denenberg (1994). Human corpus callosum: A stable mathematical model of regional neuroanatomy. *Brain and Cognition*, Vol. 25, pp. 52-66.

[8] C. Davatzikos, M. Vaillant, S. M. Resnick, J. L. Prince, S. Letovsky, and R. N. Bryan (1996). A computerized approach for morphological analysis of the corpus callosum. *Journal of Computer Assisted Tomography*, Vol. 20, pp: 88-97.

[9] R. Duara, A. Kushch, K. Gross-Glenn, W. Barker, B. Jallad, S. Pascal, D. Loewenstein, J. Sheldon, M. Rabin, B. Levin and H. Lubs (1991). Neuroanatomic differences between dyslexic and normal readers on magnetic resonance imaging scans. *Archives of Neurology*, Vol. 48, pp. 410-416.

[10] J. Duncan, Y. Wang, A. A. Amini, R. Greene, L. Kier, J. Gore, J. Holahan, S. Shaywitz, J. Fletcher, R. Bronen, and B. Shaywitz (1996). An MRI-based study of the corpus callosum in dyslexic and normal children. *Neurology*.

[11] N. Duta and M. Sonka (1998). Segmentation and interpretation of MR brain images: An improved active shape model. *IEEE Transcations on Medical Imaging*, Vol. 17, pp. 1049-1062.

[12] J. Feldmar and N. Ayache (1996). Rigid, affine and locally affine registration of free-form surfaces. *Int. J. of Comp. Vision*, Vol. 18, pp. 99-119.

[13] A. Ghanei, H. Solitanian-Zadeh and J. P. Windham (1998). Segmentation of the hippocampus from brain MRI using deformable contours. *Computerized Medical Imaging and Graphics*, Vol. 22, pp. 203-216.

[14] C. Goodall (1991). Procrustes methods in the statistical analysis of shape. *Journal of the Royal Statistical Society, Series B*, Vol. 53, pp. 285-339.

[15] H. Hampel, S. J. Teipel, G. E. Alexander, B. Horwitz, D. Teichberg, M. B. Schapiro, and S. I. Rapoport (1998). Corpus callosum atrophy is a possible indicator of region- and cell type-specific neuronal degeneration in Alzheimer disease. *Archives of Neurology*, Vol. 55, pp. 193-198.

[16] J. Haslett (1985). Maximum likelihood discriminant analysis on the plane using a Markovian model of spatial context. *Pattern Recognition*, Vol. 18, pp. 287-296.

[17] M. Holden, E. Steen, and A. Lundervold (1995). Segmentation and visualization of brain lesions in multispectral magnetic resonance images. *Computerized Medical Imaging and Graphics*, Vol. 19, pp. 171-183.

[18] G. W. Hynd, J. Hall, E. S. Novey, D. Eliopulos, K. Black, J. J. Gonzalez, J. E. Edmonds, C. Riccio, and M. Cohen (1995). Dyslexia and corpus callosum morphology. *Archives of Neurology*, Vol. 52, pp. 32-38.

[19] A. K. Jain and R. C. Dubes (1988). *Algorithms for Clustering Data*. Prentice-Hall, New Jersey.

[20] A. Lundervold, A. Fenstad, L. Ersland, and T. Taxt (1996). Brain tissue volumes from multispectral 3D MRI - A comparative study of four classifiers. In *Proceedings of the Fourth Meeting of the International Society of Magnetic Resonance in Medicine*, page 33, New York, USA, April 27 - May 3 1996.

[21] A. Lundervold and G. Storvik (1995). Segmentation of brain parenchyma and cerebrospinal fluid in multispectral magnetic resonance images (1995). *IEEE Transcations on Medical Imaging*, Vol. 14, pp. 339-349.

[22] A. Lundervold, T. Taxt, L. Ersland and A. M. Fenstad (1998). Volume distribution of cerebrospinal fluid using multispectral MR imaging. Submitted to *Medical Image Analysis*.

[23] I. K. Lyoo, A. Satlin, C. K. Lee and P. F. Renshaw (1997). Regional atrophy of the corpus callosum in subjects with Alzheimer's disease and multi-infarct dementia. *Psychiatry Research*, Vol. 74, pp. 63-72.

[24] T. McInerney and D. Terzopoulos (1996). Deformable models in medical image analysis: a survey. *Medical Image Analysis*, Vol. 1, pp. 91-108.

[25] A. Neumann and C. Lorenz (1998). Statistical shape model based segmentation of medical images. *Computerized Medical Imaging and Graphics*, Vol. 22, pp. 133-143.

[26] S. V. Raman, S. Sarkar and K. L. Boyer (1993). Hypothesizing structures in edge-focused cerebral magnetic resonance images using graph-theoretic cycle enumeration. *CVGIP: Image Understanding*, Vol. 57, pp. 81-98.

[27] R. A. Rauch and J. R. Jinkins (1996). Variability of corpus callosal area measurements from midsagittal MR images: effect of subject placement within the scanner. *American Journal of Neuroradiology*, Vol. 17, pp. 27-28.

[28] J. M. Rumsey, M. F. Casanova, G. B. Mannheim, N. Patronas, N. DeVaughn, S. D. Hamburger and T. Aquino (1996). Corpus callosum morphology, as measured with MRI, in dyslexic men. *Biological Psychiatry*, Vol. 39, pp. 769-775.

[29] D. Salat, A. Ward, J. A. Kaye and J. S. Janowsky (1997). Sex differences in the corpus callosum with aging. *Neurobiology of Aging*, Vol. 18, pp. 191-197.

[30] M. Semrud-Clikeman, P. A. Filipek, J. Biederman, R. Steingard, D. Kennedy, P. Renshaw and K. Bekken (1994). Attention-deficit hyperactivity disorder: magnetic resonance imaging morphometric analysis of the corpus callosum. *Journal of American Academy of Child and Adolescent Psychiatry*, Vol. 33, pp. 875-881.

[31] L. H. Staib and J. S. Duncan (1992). Boundary finding with parametrically deformable models. *IEEE Trans PAMI*, Vol. 14, pp. 1061-1075.

[32] G. Szekely, A. Kelemen, C. Brechbuhler, and G. Gerig (1996). Segmentation of 2-D and 3-D objects from MRI volume data using constrained elastic deformations of flexible Fourier contour and surface models. *Medical Image Analysis*, Vol. 1, pp. 19-34.

[33] J. Talairach and P. Tournox (1988). *Co-planar stereotaxic atlas of the human brain*, Thieme.

[34] T. Taxt, A. Lundervold, B. Fuglaas, H. Lien, and V. Abeler (1992). Multispectral analysis of uterine corpus tumors in magnetic resonance imaging. *Magnetic Resonance in Medicine*, Vol. 23, pp. 55-76.

[35] T. M. Taxt and A. Lundervold (1994). Multispectral analysis of the brain using magnetic resonance imaging. *IEEE Transactions on Medical Imaging*, Vol. 13, pp. 470-481.

[36] B. C. Vemuri, Y. Guo, C. M. Leonard, S-H. Lai (1997). Fast numerical algorithms for fitting multiresolution hybrid shape models to brain MRI. *Medical Image Analysis*, Vol. 1, pp. 343-362.

[37] S. Weis, M. Kimbacher, E. Wenger, and A. Neuhold (1993). Morphometric analysis of the corpus callosum using MRI: Correlation of measurements with aging in healthy individuals. *American Journal of Neuroradiology*, Vol. 14, pp. 637-645.

[38] C. Xu and J. L. Prince (1998). Snakes, shapes, and gradient vector flow. *IEEE Trans Image Processing*, Vol. 7, pp. 359-369.